3-D wave-equation prestack imaging under salt

Biondo Biondi, Louis Vaillant, Stanford University*

ABSTRACT

Wave-equation migration methods can overcome some of the limitations of Kirchhoff migration when imaging subsalt reflectors. Offset plane wave migration and common-azimuth migration are among the most promising wave-equation migration methods for efficiently imaging 3-D marine data sets. Offset plane wave migration has some computational advantages over common-azimuth migration, but subsalt images produced by common-azimuth migration are better focused than the corresponding images produced by our implementation of offset plane wave migration. A theoretical and a numerical analysis demonstrate the advantages and limitations of the common-azimuth approximation when estimating the cross-line component of the offset ray parameter vector from common-azimuth data, as compared with setting this component to zero.

INTRODUCTION

Kirchhoff migration methods often fail to produce satisfactory images of reflectors below complex overburden because they do not handle correctly multipathing of the reflected energy. When the wavefield is severely distorted by a salt body, or other complex velocity structure, the computation of the multivalued Green functions required by Kirchhoff methods is challenging. Further, even if we were able to compute the Green functions accurately and efficiently, the numerical integration of the wavefield over patchy and multivalued integration surfaces would be a difficult, and probably unreliable, task.

Wave-equation methods are an attractive and robust alternative to the complexities involved in extending Kirchhoff migration to handle correctly multipathing. However, full wave-equation 3-D prestack migration is still too computationally intensive to become a practical tool. Therefore, in the past few years we developed common-azimuth migration that is an approximation to full wave-equation 3-D prestack migration (Biondi and Palacharla, 1996). It exploits the narrow-azimuth nature of marine data to reduce the computational cost by a large factor (20 to 50) with respect to full wave-equation 3-D prestack migration. In another abstract (Vaillant et al., 2000) we show that common-azimuth prestack migration produces better images than a state of the art Kirchhoff migration for a salt body in the North Sea. The evidence is mounting that wave-equation migration, even when applied using approximate methods as common-azimuth, has the potential to produce better images than Kirchhoff methods when strong lateral velocity variations cause multi-pathing of the reflected energy. Full-volume imaging of deep targets when steep reflectors require huge migration aperture is another area of applications for efficient wave-equation migration methods that is gaining interest. In these cases the cost of Kirchhoff migration is large, and downward continuation methods become computationally attractive.

Offset plane wave migration (Ottolini and Claerbout, 1984; Mosher et al., 1997) is another approximate wave-equation method that has been recently applied to the migration of 3-D prestack marine data. Offset plane wave migration is related to common-azimuth migration, and has similar computational complexity. Both methods achieve computational efficiency by restricting the computational domain to a 4-D space from the 5-D space that is required by full downward continuation. Offset plane wave migration reduces the dimensionality of the computational domain by first decomposing the data into offset plane waves, and then downward continuing and imaging each offset plane wave independently. Offset plane wave migration has the additional computational advantage that it can be performed as several independent migrations of 3-D cubes, while common-azimuth migration requires, at least in principle, to be performed on the whole 4-D data set simultaneously. This difference means that offset-plane wave migration requires less computations (about 10%) and has lower minimum-memory requirements to run efficiently. However, for both methods the memory requirements are manageable on modern computers because the computational domain is further decomposed in temporal-frequency components. On the other hand, downward continuing the offset plane waves separately introduces errors when migration velocity has strong lateral variations, as in the case of subsalt imaging. In this paper we show examples of migration errors related to this approximation when imaging the narrow-azimuth subset of SEG-EAGE salt model (known as C3 Narrow-Azimuth classic data set or C3-NA)

EFFICIENT WAVE-EQUATION MIGRATIONS

The full downward continuation of 3-D prestack data can be performed in the frequency-wavenumber domain by applying the Double Square Root (DSR) phase-shift operator

$$\begin{aligned} k_z &= \sqrt{\frac{\omega^2}{v^2(\mathbf{s},z)} - \frac{1}{4}\left[\left(k_{x_m}-k_{x_h}\right)^2+\left(k_{y_m}-k_{y_h}\right)^2\right]} \\ &+ \sqrt{\frac{\omega^2}{v^2(\mathbf{g},z)} - \frac{1}{4}\left[\left(k_{x_m}+k_{x_h}\right)^2+\left(k_{y_m}+k_{y_h}\right)^2\right]}, \quad (1) \end{aligned}$$

where ω is the temporal frequency, $\mathbf{k_m}$ is the midpoint-wavenumber vector, $\mathbf{k_h}$ is the offset-wavenumber vector, $v(\mathbf{s},z)$ and $v(\mathbf{g},z)$ are respectively the velocity at the source and receiver locations, and we define x as the in-line direction and y as the cross-line direction. The DSR operator is a function of the cross-line component of the offset wavenumber k_{y_h}, while common-azimuth data are independent from k_{y_h} because they are different from zero only at $y_h = 0$. The exact full downward continuation is thus performed by applying a 5-D operator on a data set that is only 4-D. While accurate, this procedure is tremendously wasteful of computational efforts, because only a small subset of the 5-D wavefield contributes to the final image, which is obtained by extracting the zero-offset cube from the downward-continued wavefield. This data extraction is equivalent to the summation of the wavefield along both offset-wavenumber axes. Most of the wavefield components destructively interfere in the imaging step. In fact, only a 4-D slice of the 5-D wavefield contributes to the image when no multipathing occurs, such as in constant velocity or in a vertically layered media. Even when multipathing occurs, most of the wavefield components destructively interfere in the imaging step. It is therefore natural to limit the computational cost by reducing the dimensionality of the downward continuation operator from 5-D to 4-D. Both common-azimuth migration and offset plane wave migration achieve this goal, though in different ways. Common azimuth migration reduces the dimensionality of the continuation operator by restricting the wavefield to be common-azimuth at every depth level. This geometric condition is equivalent to selecting one particular value for the cross-line component of the offset wavenumber k_{y_h}. This value for k_{y_h} is then substituted into the expression for the full DSR of equation (1), to obtain the common-azimuth downward-continuation operator. The analytical expression for k_{y_h} can be either obtained by geometric considerations or by a stationary-phase analysis, and is given as

$$\widehat{k_{y_h}} = k_{y_m}\frac{\sqrt{\frac{\omega^2}{v^2(\mathbf{g},z)} - \frac{1}{4}\left(k_{x_m}+k_{x_h}\right)^2} - \sqrt{\frac{\omega^2}{v^2(\mathbf{s},z)} - \frac{1}{4}\left(k_{x_m}-k_{x_h}\right)^2}}{\sqrt{\frac{\omega^2}{v^2(\mathbf{g},z)} - \frac{1}{4}\left(k_{x_m}+k_{x_h}\right)^2} + \sqrt{\frac{\omega^2}{v^2(\mathbf{s},z)} - \frac{1}{4}\left(k_{x_m}-k_{x_h}\right)^2}}. \quad (2)$$

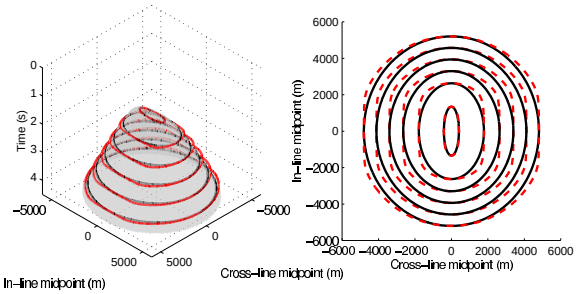

Figure 1: The grey surface shown in the left panel is the exact summation surface to image a diffractor at 500 m depth from data at a constant offset of 4,000 m, and assuming a constant velocity of 2,500 m/s. The solid contour lines correspond to the exact summation surface, while the dashed contour lines correspond to the approximate summation surface obtained by setting $p_{y_h} = 0$.

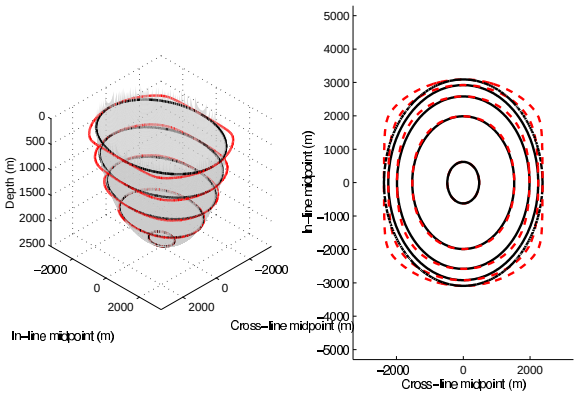

Figure 2: The grey surface shown in the left panel is the exact spreading surface for an impulse at at 2.5 s, an offset of 4,000 m, and assuming a constant velocity of 2,500 m/s. The solid contour lines correspond to the exact spreading surface, while the dashed contour lines correspond to the approximate spreading surface obtained by setting $p_{y_h} = 0$.

While equation (2) can be applied with variable velocities, it is strictly valid only in constant velocity (Biondi and Palacharla, 1996). In this paper we show that in layered medium with strong vertical gradient the errors introduced are small.

It is important to notice that common-azimuth migration can handle events emerging at the surface with non-zero cross-line component of the offset ray parameter vector $p_{y_h} = k_{y_h}/\omega$. These component of the step out in the data is estimated from the other step-out components and the local velocities using equation (2). In this section we discuss the errors when these dependencies are neglected and p_{y_h} is set equal to zero. We first analyze the errors in the simple case of constant velocity, and then show migration results of a synthetic data recorded over a horizontally layered medium.

It can be analytically demonstrated (Biondi, 1999) that neglecting the cross-line component of the offset plane wave ray parameter vector is equivalent to reversing the correct order of two-pass migration. The correct order for two-pass prestack migration is: in-line prestack migration followed by cross-line zero-offset migration (Rosa et al., 1999). On the contrary, setting $p_{y_h} = 0$ is equivalent to performing a cross-line zero offset migration followed by an in-line prestack migration.

Figure 1 provides an intuitive understanding of the approximations involved in reversing the order of the migrations. The grey surface shown in the left panel of Figure 1 is the summation surface that should be used to image a diffractor at 500 m depth from data at a constant offset of 4,000 m, and assuming a constant velocity of 2,500 m/s. Two sets of contour lines are superimposed onto the surface. The inner set of contour lines corresponds to the exact summation surface, while the outer one corresponds to the surface defined by reversing the correct order of two-pass migration. The right panel of Figure 1 shows the same contour lines in plane view. The solid lines correspond to the exact summation surface, while the dashed lines correspond to the approximate summation surface. Figure 1 graphically demonstrates that even in constant velocity setting $p_{y_h} = 0$ introduces an error for reflectors that are not exactly dipping in either the in-line direction or the cross-line direction.

The analysis of the impulse responses, or spreading surfaces, provides an alternative perspective to the analysis of the migration errors. Figure 2 compares the exact impulse response of 3-D prestack migration and the approximate one. The grey surface shown in the left panel of Figure 2 is the exact spreading surface for an impulse recorded at 2.5 s, at an offset of 4,000 m, and assuming a constant velocity of 2,500 m/s. The inner set of contour lines corresponds to the exact summation surface, while the outer one corresponds to the surface defined by reversing the correct order of two-pass migration. The right panel of Figure 2 shows the same contour lines in plane view. The solid lines correspond to the exact spreading surface, while the dashed lines correspond to the approximate spreading surface. It is apparent that the approximation is worse for shallow reflectors dipping at 45 degrees with respect to the acquisition axes. At zero offset the order of the in-line and cross-line migrations is obviously irrelevant; it is intuitive that the errors introduced by reversing the correct migration order increases with offset.

Figure 3 and 4 show the images obtained by migrating a common-azimuth synthetic data set recorded over a horizontally layered medium with a strong velocity gradient ($v(z) = 1.5$ km/s $+ 1$ s^{-1}). The maximum data offset was 5.8 km. Figure 3 was obtained using common-azimuth migration; that is, by using equation (2) to estimate p_{y_h}. Figure 4 was obtained setting $p_{y_h} = 0$. There are five dipping reflectors, dipping at 0, 30, 45, 60, and 75 degrees, and oriented at 45 degrees with respect to the acquisition axes. As discussed above, the 45 degrees orientation is the worst case for the errors introduced by setting $p_{y_h} = 0$, but it is also the worst case for the errors introduced by the common-azimuth approximation (Biondi and Palacharla, 1996). The front panel in both figures shows an in-line section of the migrated cube. The side and top panels show respectively a vertical and a horizontal section of the angle-domain Common Image Gathers (CIG). Common-azimuth migration introduced rather small errors even for the steeply dipping reflectors and large reflection angles (i.e. large offset). On the contrary, the steeply dipping reflectors (60 and 75 degrees) are poorly imaged when p_{y_h} is set equal to zero.

SUBSALT MIGRATION RESULTS

In this section we analyze the migration results obtained on the Salt Model C3-NA data set by Kirchhoff migration, offset plane wave migration, and common-azimuth migration. The Kirchhoff program implemented a single-arrival Kirchhoff migration. The wave-equation migrations operated on data transformed to effective common-azimuth data by applying Azimuth Moveout (Biondi et al., 1998). Both offset plane waves and common-azimuth migrations were implemented a frequency-wavenumber domain algorithm, adapted to lateral velocity variations by an extended split-step method (Stoffa et al., 1990) using six reference velocities.

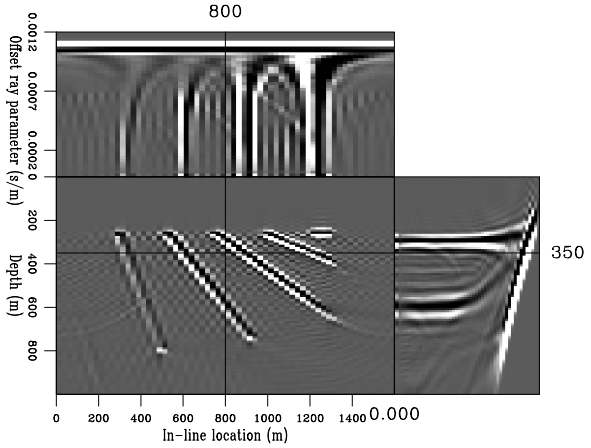

Figure 3: Common-azimuth migration of synthetic data.

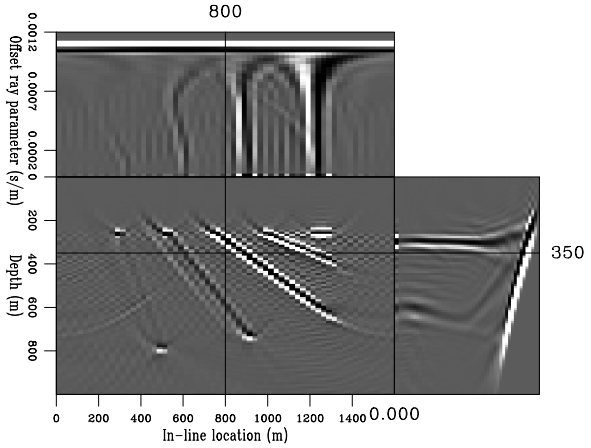

Figure 4: Migration of synthetic data obtained by setting $p_{y_h} = 0$.

Figure 5 shows a cross-line section of the lower part of the velocity cube. This cross-line section passes through the two subsalt sand lenses. It cut through one of the most challenging areas in the model, where the top of the salt body has deep indentations. The steep flanks of the canyons, and the large velocity contrast between the salt body and the soft sediments filling the canyons, cause a severe distortion of the reflected wavefield. The bottom of the salt and the reflectors below, including the basement, are thus poorly illuminated.

Figures 6a, 6b, and 6c, show the cross-line sections through the full-volume 3-D prestack migration cube obtained respectively by Kirchhoff migration (a), offset plane wave migration (b), and common-azimuth migration (c). The wave-equation images are superior to the Kirchhoff image in several ways. First, the wave-equation images lack the strong coherent artifacts that makes the Kirchhoff image difficult to interpret. These artifacts are caused by partially coherent stacking of multipathing events along wrong trajectories. They are typical of Kirchhoff subsalt images, and can be only partially removed by a "smart" selection of the Kirchhoff summation surfaces, such as the ones suggested by the most-energetic arrival or shortest-path. In the column below the canyons, the Kirchhoff image shows strong artifacts that could be easily interpreted as reflections. Second, both lenses are interpretable from the common-azimuth image while in the Kirchhoff image they are either lost in the noise (top lens) or completely missing (bottom lens). Third, both the bottom of the salt and the basement are more continuous in the wave-equation images.

Comparing the two wave-equation images we notice that offset-plane waves is not as accurate as common-azimuth migration because of the strong lateral velocity variations caused by the salt body. The approximation introduced by downward-continuing the offset plane wave separately causes significant problems in the imaging of the sub-salt reflectors. Both sand lenses visible in the right part of the sections are better imaged by common-azimuth migration (c) than by offset-plane wave migration (b). Though discontinuous in places, the basement reflector is also better imaged in (c) than in (b). The bottom of the salt reflector right below the deep canyons in the salt body (in-line location 8,000-9,200 m) is fairly coherent in panel (c), while it is discontinuous in panel (b).

CONCLUSIONS

Wave-equation migrations produced better results in the subsalt than a single-arrival Kirchhoff migration. The subsalt reflectors are much more interpretable in the wave-equation images than in the Kirchhoff images, both because the images are devoid of the typical subsalt Kirchhoff artifacts and because the reflectors themselves are better imaged.

The images produced by common-azimuth migration are better focused than the images produced by our implementation of offset plane wave migration. These differences can be attributed to an approximation intrinsic to offset plane wave migration: the offset plane wave components are downward continued separately, instead of being allowed to mix as they should be in media with laterally varying velocity.

ACKNOWLEDGMENTS

We would like to thank Mihai Popovici at 3DGeo Development Inc. for providing us the Kirchhoff migration images shown in the paper. The first author (B.B.) would like also to thank Chuck Mosher with Arco for many enlightening conversations on offset plane wave migration.

REFERENCES

Biondi, B., and Palacharla, G., 1996, 3-D prestack migration of common-azimuth data: Geophysics, **61**, 1822–1832.

Biondi, B., Fomel, S., and Chemingui, N., 1998, Azimuth moveout for 3-D prestack imaging: Geophysics, **63**, no. 2, 574–588.

Biondi, B., 1999, Offset plane waves vs. common-azimuth migration for sub-salt imaging: SEP–**102**, 15–34.

Mosher, C. C., Foster, D. J., and Hassanzadeh, S., 1997, Common angle imaging with offset plane waves: 67th Annual Internat. Mtg., Soc. Expl. Geophys., Expanded Abstracts, 1379–1382.

Ottolini, R., and Claerbout, J. F., 1984, The migration of common-midpoint slant stacks: Geophysics, **49**, no. 03, 237–249.

Rosa, A., Cunha, C., Pedrosa, I., Panetta, J., Sinedino, S., and Braga, V., 1999, Two-pass 3-D prestack time migration: 6th Internat. Congr. Braz. Geophys. Soc., SBGf, RIO 99, CD–ROM.

Stoffa, P. L., Fokkema, J. T., de Luna Freire, R. M., and Kessinger, W. P., 1990, Split-step Fourier migration: Geophysics, **55**, no. 4, 410–421.

Vaillant, L., Calandra, H., Sava, P., and Biondi, B., 2000, 3-D wave-equation imaging of a North Sea dataset: common-azimuth migration + residual migration: 70th Annual Internat. Mtg., Soc. Expl. Geophys., Expanded Abstracts, submitted.

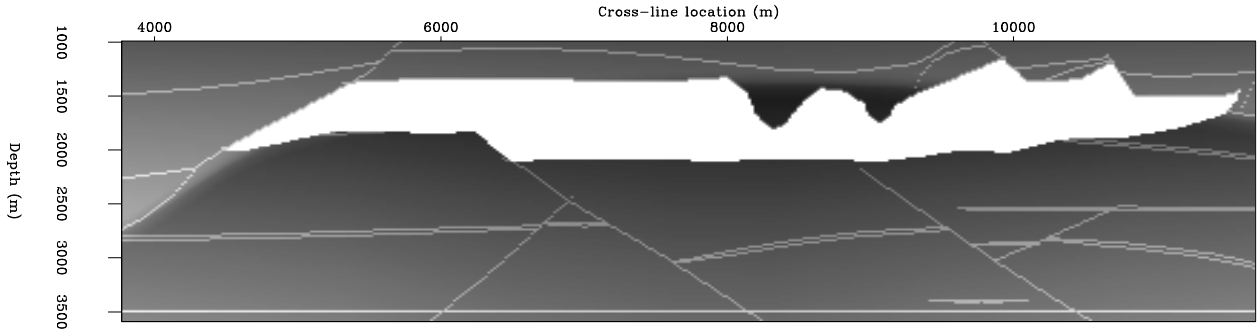

Figure 5: Velocity model at constant cross-line coordinate y=7.5 km.

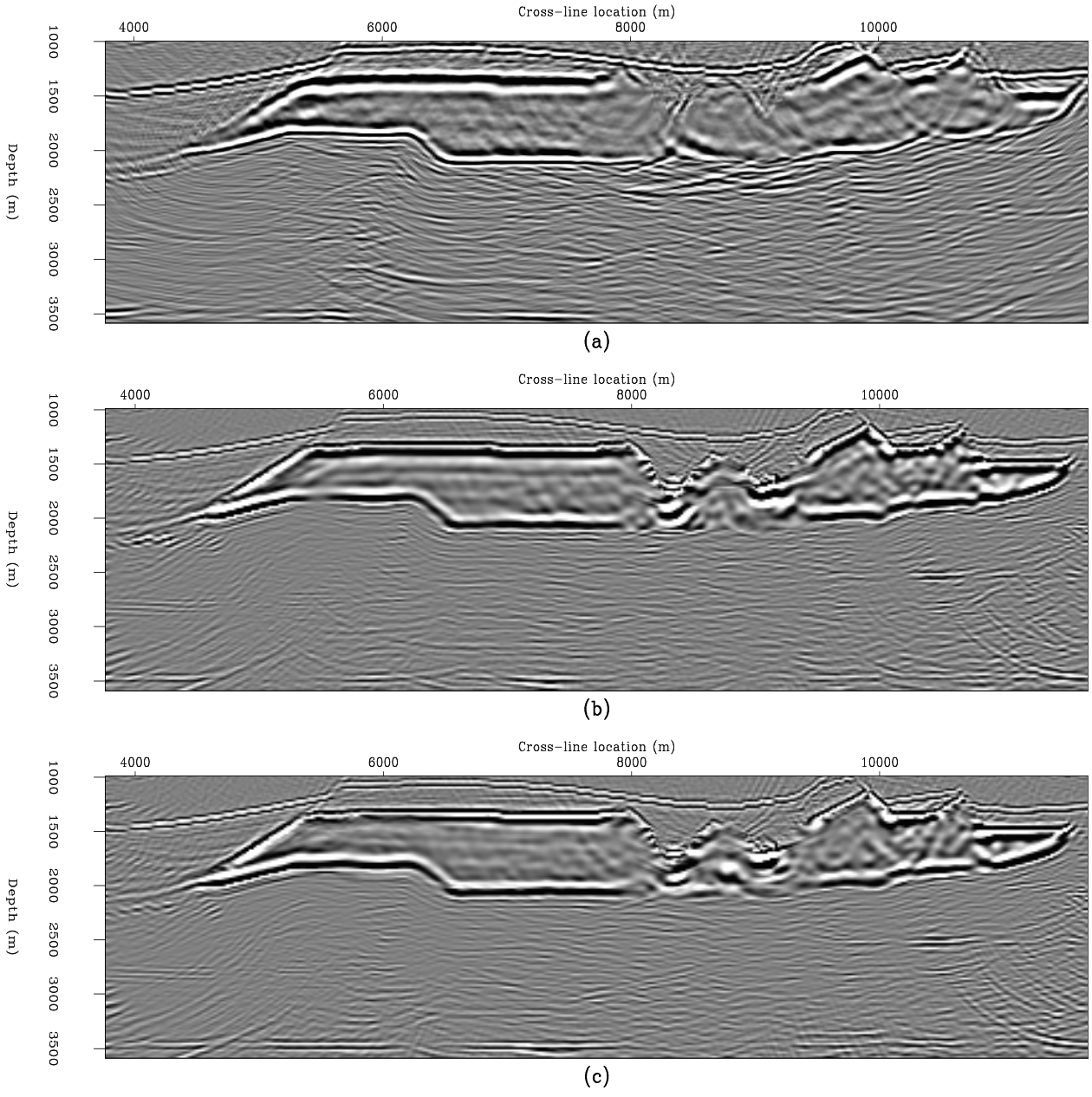

Figure 6: Kirchhoff migration (a), offset plane wave migration (b), and common-azimuth migration (c), at constant cross-line coordinate y=7.5 km. All three sections are rendered using the same percentile for clipping amplitudes.